Journal of Luminescence 231 (2021) 117802

Contents lists available at ScienceDirect

Journal of Luminescence

journal homepage: http://www.elsevier.com/locate/jlumin

Full Length Article

Thermoluminescence of fluorapatite mineral

G.P.S. Silva [a], M.C.S. Nunes [a], C. Ulsen [b], R. Künzel [c], E.M. Yoshimura [d], N.M. Trindade [a,d,*]

[a] Department of Physics, Federal Institute of Education, Science and Technology of São Paulo, São Paulo, SP, Brazil
[b] Universidade de São Paulo – Escola Politécnica. Technological Characterization Laboratory, São Paulo, SP, Brazil
[c] Department of Physics, Federal University of São Paulo, Diadema, SP, Brazil
[d] Institute of Physics, University of São Paulo, São Paulo, SP, Brazil

ARTICLE INFO

Keywords:
Fluorapatite
Mineral
Luminescence
X-ray diffraction

ABSTRACT

Fluorapatite [$Ca_{10}(PO_4)_6F_2$] is a mineral of the apatite group of the highest occurrence in the world among phosphates. The material is known for its diverse luminescent properties, as fluorescent lamps and lasers. The thermoluminescence (TL) signal of apatite from various origins has been investigated in the past years, mainly of the Mexican origin. In this work, the objective was to investigate the TL of samples of the Brazilian natural fluorapatites submitted to beta-ionizing radiation. The chemical composition of the samples was obtained by the technique of X-ray fluorescence and the electronic transitions were verified by optical absorption in the visible region. The mineral presented a wide optical absorption band between 500 nm and 750 nm, typical of fluorapatite, and SEM/EDS showed a high percentage of purity. The registered Raman spectrum exhibits the characteristics modes from the PO_4^{3-} tetrahedra, observed in fluorapatite, and a band at 1103 cm^{-1} characteristic of the $(CaO_3)^{2-}$ carbonate group. The TL measurements were carried out using a commercial Risø TL/OSL reader, model DA-20, equipped with a built in $^{90}Sr/^{90}Y$ beta source, with different radiation doses (1–5 Gy). The TL glow curve showed three peaks located at about 350 K, 470 K and 570 K (heating rate of 1 K/s). The activation energy and the frequency factor associated with each peak were determined by different methods. In addition, the TL response (area under the peaks) has shown linear behavior in relation to the doses.

1. Introduction

The apatite supergroup is formally divided into five groups of minerals described by the general formula $^{IX}M1_4^{VII}M2_6(^{IV}TO_4)_6X_2$ [M = Ca^{2+}, Pb^{2+}, Ba^{2+}, Sr^{2+}, Mn^{2+}, Na^{+}, Ce^{3+}, La^{3+}, Y^{3+}, Bi^{3+}; T = P^{5+}, As^{5+}, V^{5+}, Si^{4+}, S^{6+}, B^{3+}, X = F^{-}, $(OH)^{-}$, Cl^{-}], that can be phosphates, arsenates, vanadates, silicates, and sulphates [1]. This general formula corresponds to the unit cell content, indicating the four key sites (M1, M2, T and X) and their coordination numbers (IX, VII and IV) [1]. However, the name "apatite" is currently used as a generic expression to refer to three calcium phosphates of this supergroup described by the simplified formula $Ca_{10}(PO_4)_6X_2$, namely hydroxyapatite (X = OH), chlorapatite (X = Cl) and fluorapatite (X = F) [2,3]. The fluorapatite crystal structure is hexagonal and belongs to the $P6_3/m(C_{6h}^2)$ spatial group [4–6].

Among the most abundant non-silicate minerals, apatite is the main source of phosphate on Earth [7–9]. In Brazil, almost all the phosphate used in industry comes from igneous origin, that is, from alkaline-carbonatite complexes. The variant containing the F^{-} anion in the anionic site (fluorapatite) [8] is the most common. In the natural form, apatite is widely used in industry, for example, in the production of detergents, insecticides, animal and human feeding [2,8]. On the other hand, the synthetic apatite presents a variety of applications, mainly as phosphors in fluorescent lamps, in the chromatographic separation of proteins and in soil decontamination with heavy metal ions [2,10], and more recently, used as a laser as well [7,11].

The minerals in the apatite group have diverse luminescent properties. According to Waychunas [11], the diversity of its luminescence has some causes such as: the ability to incorporate activators and co-activators of transition metals, for example, metallic cations that replace Ca in its structure, and anionic impurities that replace $(PO_4)^{3-}$; the varied types of associations and formation conditions that promote luminescent activity; and the apatite crystalline matrix itself. Due to the luminescent properties of apatite, this work proposes the study of fluorapatite, using the thermoluminescence (TL) technique. TL is the light emitted by some crystals when heated. It is a thermally stimulated emission of an energy that was previously stored in the crystal during irradiation, in addition to the incandescence [12]. TL materials are

* Corresponding author. Department of Physics, Federal Institute of Education, Science and Technology of São Paulo, São Paulo, SP, Brazil.
E-mail address: ntrindade@ifsp.edu.br (N.M. Trindade).

https://doi.org/10.1016/j.jlumin.2020.117802
Received 18 July 2020; Received in revised form 20 November 2020; Accepted 23 November 2020
Available online 3 December 2020

usually ionic crystals, in which the valence band is filled with electrons and the conduction band is empty, and between these bands there is an energy gap. Defects in the material can generate relatively shallow energy levels within the gap, which act as traps for charged carriers (electrons or holes). The thermal stimulation releases charge carriers from traps and their recombination at luminescence centers gives rise to the light emission [12,13]. As the charge carrier population in the traps of these luminescent materials is the result of the irradiation, TL intensities can be related to the absorbed dose [12,14].

Among the materials that present TL properties, some natural minerals as quartz [15–18], calcite [19,20], feldspar [21,22], silicates group [23,24] and, recently, alexandrite [25–29] have been investigated. Lapraz and Baumer [30] collected TL spectra from samples of natural fluorapatite from various countries. Recently, an extensive research has been carried out on Durango apatite and its anomalous fading (AF) [31–37]. Kitis et al. [34,35] have analyzed the influence of different factors on the AF in Durango apatites and concluded that it is a process of high independence degree from external parameters. Moreover, tunneling is the most probable cause of this anomalous fading, which interferes with dosimetry and dating applications. Polymeris et al. [38] have also checked the AF in apatites from different countries, including some Brazilian samples. However, to the best of our knowledge, this is the first time that a kinetic study is done for the TL emission of Brazilian fluorapatites.

2. Materials and methods

The studied mineral, blue-colored appearance, is of igneous origin with a high purity content. Fig. 1 shows a slice of the crystal cut according to the basal plane (001). The samples used presented their natural faces clean and free of defects.

The chemical and phase characterization of the sample was done by Scanning Electron Microscopy (SEM) and Chemical Microanalysis by Dispersive Energy Spectroscopy (EDS). EDS analysis was performed using an INCA microanalysis system (Oxford Instruments) in conjunction with a Leo 440 Stereo scan SEM. To identify the crystalline phases in the sample, an X-Ray Diffraction analysis was performed using a Philips X'PERT-MPD equipment (45 kV- 40 mA operating power), Cu Kα radiation (1.5405 Å), in the 2θ range between 2° and 70°. The identification of the crystalline phases was obtained by comparing the sample diffractogram with the PDF4 databases of the ICDD - International Center for Diffraction Data and ICSD - Inorganic Crystal Structure Database using the software HighScore Plus from Malvern Panalytical.

In addition, to investigate the defects and impurities related to the luminescent properties of the fluorapatite sample, the optical absorption (OA) spectrum of the material was obtained. For this measurement, a SHIMADZU UV-2600 spectrophotometer in the range 400 nm–800 nm and spectral resolution of 0.5 nm was used. The optical absorption data were obtained indirectly by the reflectance of the sample. Furthermore, the Raman spectrum was registered using a Raman Renishaw microscope (in Via model) with a CCD detector and He–Ne laser (632.8 nm), set to 0.17 mW at the sample. The data were registered in the range from 20 to 1250 cm^{-1} using the automatic cosmic ray removal option. The instrumental Raman shift was calibrated using 520.5 cm^{-1} line of a Silicon standard. To adjust the sample in the TL equipment and to ensure homogeneity in the results, the crystal was pulverized and sieved to grains smaller than 0.075 mm. Besides the TL measurements a sample with this grain size was used for the optical absorption measurements. For structural analysis, powder was also used, however with grains smaller than 0.040 mm. On the other hand, for chemical analysis the sliced fluorapatite sample was used.

The sample was heated at 20 K/min up to 773 K in a muffle furnace and kept at this temperature for 1 h to erase the effects of natural irradiation. Then, the sample was cooled at 20 K/min down to room temperature. Irradiation was performed at room temperature using the built-in $^{90}Sr/^{90}Y$ beta source (dose rate of 10 mGy/s) inside the TL equipment. TL measurements were carried out using a commercial automated TL/OSL reader made by Risø National Laboratory (model DA-20). TL glow curves were obtained using a heating rate of 1 K/s, from RT to 773 K. The experiments described below were performed immediately after the beta irradiation to avoid the influence of fading of the TL peaks. The TL signal was detected with a bialkali photomultiplier tube behind an UV-transmitting and visible-absorbing glass filter (Hoya U-340, 7.5 mm thick). The extraction of the kinetic parameters and the analysis of the glow curves involved several methods, as T_m-T_{stop}, T_m as a function of irradiation dose (dose range from 1 to 5 Gy), peak shape of the TL glow curve, and glow curve fitting methods.

3. Results and discussion

Fig. 2 shows the XRD patterns of the fluorapatite, in blue, and the diffraction lines corresponding to the database, in red, indicating a pattern consistent with fluorapatite (ICDD: 04-011-3604) with the three most intense peaks at 31.92° (d = 2.80 Å, plane 211), 32.25° (d = 2.77 Å, plane 112) and 33.09° (d = 2.70 Å, plane 300), which mineral composition was also confirmed by SEM/EDS chemical analysis. The observed diffraction peaks can be indexed to the hexagonal $Ca_{10}(PO_4)_6F_2$ structure and $P6_3/m$ symmetry group [5].

The SEM-backscattered (BSE) image (Fig. 3) reveals homogeneity of the gray levels in the image, indicating homogeneity in chemical composition and confirming the existence of a single mineral. The chemical composition (average weight percentages of elements) of the studied fluorapatite sample assessed by SEM/EDS is shown in Table 1. According to Miler and Mirtič [39], the general relative standard deviation of EDS measurements is in the order of 8% for polished samples. This result in Table 1 is characteristic of fluorapatite [40], and indicates a highly pure crystal containing low percentage of impurities (Si and S) in its composition. In addition to the chemical elements typical of

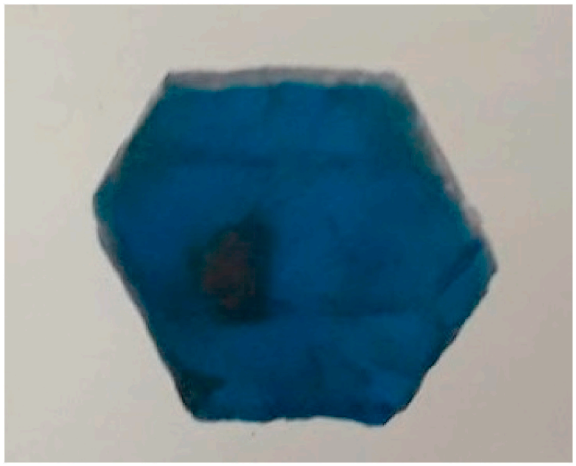

Fig. 1. Sliced natural fluorapatite.

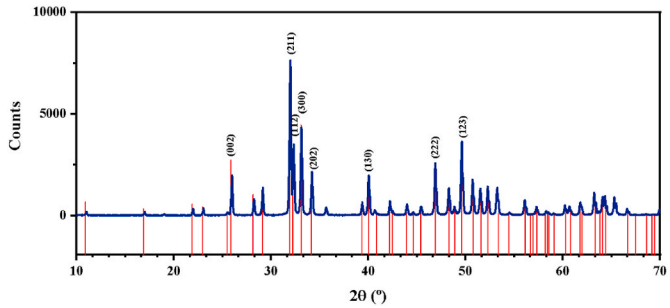

Fig. 2. X-ray diffraction (XRD) spectrum of natural fluorapatite.

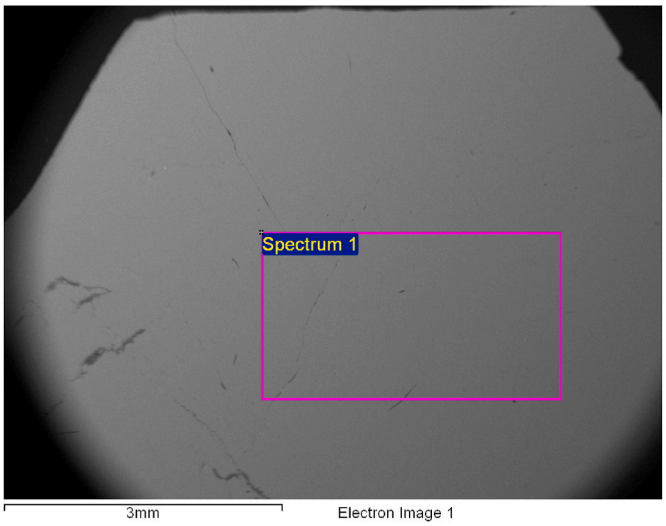

Fig. 3. Scanning electron microscope backscattered (SEM-BSE) image of fluorapatite.

Table 1
EDS results of the fluorapatite sample composition, in wt%.

F	Si	P	S	Ca	O
3.80	0.45	18.0	0.57	37.7	39.5

fluorapatite, oxygen (O), fluorine (F), phosphate (P) and calcium (Ca), it is common to find in natural samples substitutions by metal ions (*e.g.*, Mn, Fe, Ti and Cr) and rare earths (*e.g.*, Ce, Pr, Nd, Sm, Er, Tm and Eu) [40,41]. This large variety of impurities, for example, makes it difficult to define the elements responsible for the color in apatite [40]. Nonetheless, due to an experimental limitation, EDS cannot detect the lightest elements and elements with low concentration, therefore, in this work, no manganese or any rare earth was found, although other authors [40, 41] have pointed out the presence of traces of these elements.

Fig. 4 shows the optical absorption spectrum of the fluorapatite sample. The wide band in the visible spectrum at 550–700 nm is associated with the presence of manganese ions. According to Ribeiro et al. [40], a band centered at 610 and 650 nm assigned to $(MnO_4)^{3-}$ substituting for $(PO_4)^{3-}$ or Mn^{5+} ions is expected in the optical absorption spectrum of Brazilian blue-green fluorapatites. A Mn concentration as low as 0.04% produces OA peaks as high as the one observed in this work [40]. The replacement of calcium by Mn^{2+} ions, also common in apatites, can be identified in the optical absorption spectrum with the presence of characteristic band in 600 nm [42] as well. However, according to Gilinskaya et al. [41], the blue color of natural apatite is due to $(SO_3)^-$ transitions that also appear in the visible spectrum at 600 nm. As our sample presents $(SO_3)^-$, and traces of Mn might not be detected in the EDS analysis, both hypotheses are feasible to explain the wide OA band. In addition to the bands already described, a low intensity peak at 740 nm is seen in Fig. 4. This peak is due to the presence of Nd^{3+}, a rare earth ion that also is related to a peak at 800 nm, due to $^4I_{9/2} \rightarrow {}^4F_{7/2}$, $^4S_{3/2}$ and $^4I_{9/2} \rightarrow {}^4F_{5/2}$, $^2H_{9/2}$ electronic transitions [2,43].

Fig. 5 depicts the Raman spectrum of natural fluorapatite powder over the 100 to 1250 cm^{-1} wavenumber range. The observed peaks are mainly related to the $[PO_4]^{3-}$ tetrahedra lattice vibrations observed in fluorapatite [44–46]. The peak observed at 962 cm^{-1} is assigned to the ν_1 ($[PO_4]^{3-}$) symmetric stretching [46]. In the ν_4 ($[PO_4]^{3-}$) bending mode, three peaks are at 580, 590, and 606 cm^{-1} [44]. The peaks located at 1063 cm^{-1} correspond to the ν_3 ($[PO_4]^{3-}$) anti-symmetric stretching vibration [44]. The peak at 430 cm^{-1} relates to the ν_2 ($[PO_4]^{3-}$) bending vibration mode. The low-frequency bands observed at 137 cm^{-1} and 112 cm^{-1} correspond to external modes from the ($[PO_4]^{3-}$) ions [44]. The weak band located at 1008 cm^{-1} is assigned to the hydroxy-fluorapatite ν_1 ($[HPO_4]^{2-}$) vibration [46]. The strong Raman peak located at 1103 cm^{-1} can be assigned to the ν_1 mode from the carbonate group $(CaO_3)^{2-}$. This substitution of carbonate ions induces the creation of vacancies and distortions in the material lattice structure [45,46].

To obtain the thermoluminescence signal from the sample of fluorapatite, an aliquot (~40 mg) of the powdered sample was irradiated (doses from 1 to 5 Gy) and immediately readout at a heating rate of 1 K/s. After each TL readout, and before the following irradiation, the sample was heated to 653 K, at a heating rate of 5 K/s, in order to clean the residual signal. The glow curves of this fluorapatite sample are shown in Fig. 6, and it is possible to identify three peaks, at ~350 K, ~470 K and ~570 K, labeled peaks I, II and III, respectively. There are no noticeable changes in the TL glow curve shapes in this interval of doses. It is interesting to note that the peak of highest intensity appears at the lowest temperature, as observed by Ekendahl et al. [47] on the TL properties of a fluorapatite sample coated with a glass-ceramic

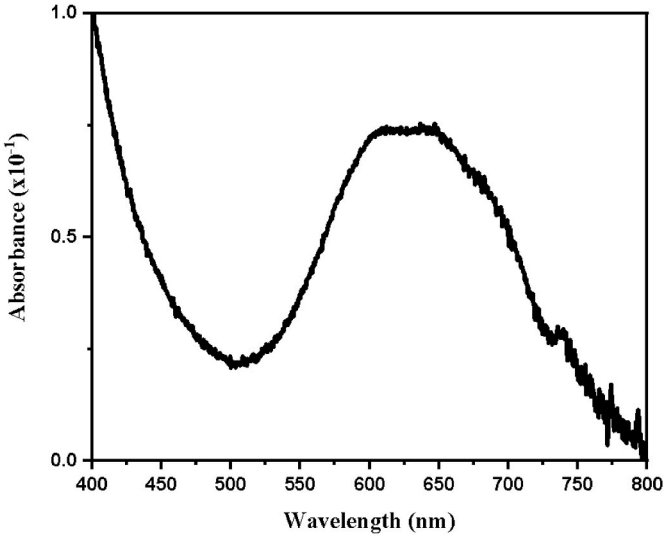

Fig. 4. Visible and near infrared optical absorption from fluorapatite crystal.

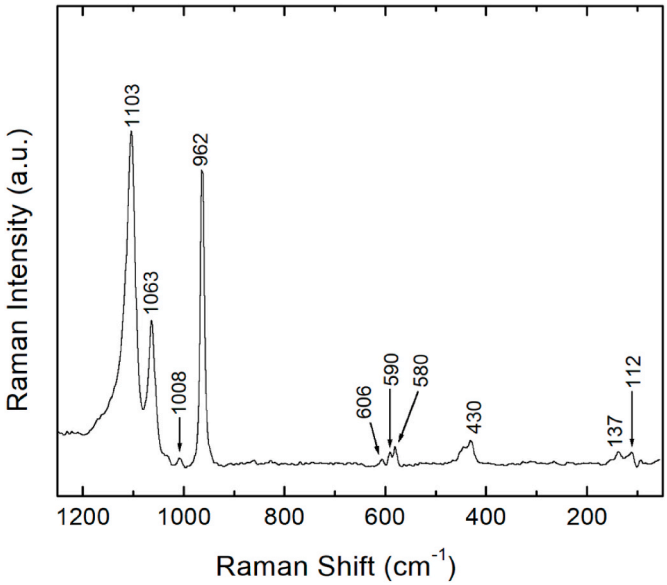

Fig. 5. Raman spectrum of fluorapatite sample.

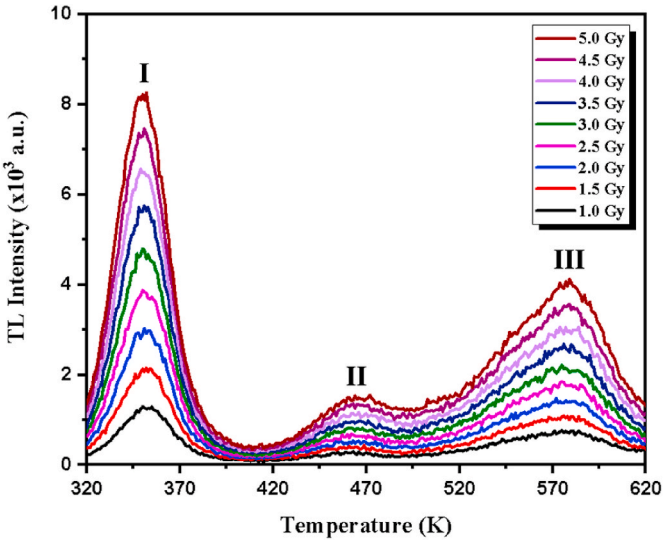

Fig. 6. TL glow curves of fluorapatite powdered sample for various radiation doses.

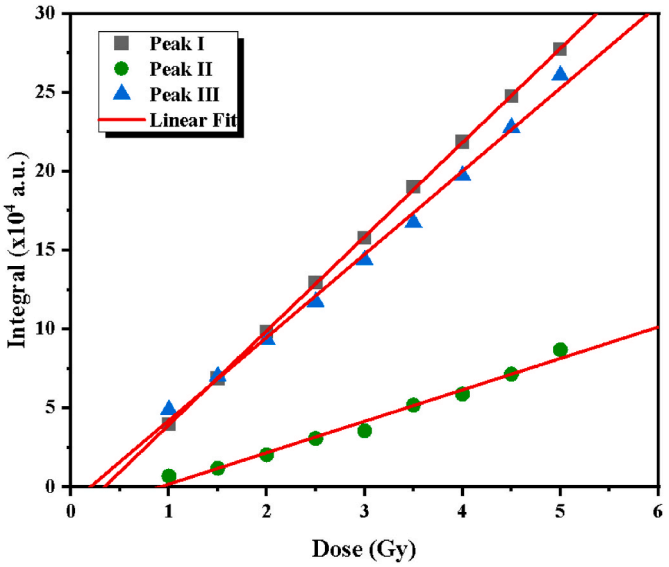

Fig. 7. Area under the peaks observed in the TL glow curve of fluorapatite as a function of the radiation dose.

compound, using beta radiation and a dose of 5 Gy. They also identified three TL peaks, however, at different positions compared to those observed here: at 5 K/s, the observed peak temperatures were ~370 K, ~440 K and ~550 K. Tsirliganis et al. [32] showed that Durango apatite presents two glow peaks at ~ 470 K and ~590 K (5 K/s). Evaluating the thermoluminescence response of apatites from different countries, Polymeris et al. [38] has identified two peaks at ~ 400 K and ~500 K on the glow curve of Brazilian fluorapatites (heating rate of 1 K/s). In addition, it was possible to verify the ubiquitous AF in all fluorapatite samples [38]. Lapraz and Baumer [30] did a comprehensive study on the TL of natural and synthetic fluorapatites, doped with various activators. They concluded that the trapping centers for all the crystals are related to intrinsic defects, as the peak positions do not change with the type of dopant. In fact, they suggest that O^{2-} vacancies on halide sites connected to $(PO_4)^{3-}$ act as trapping centers. These centers were identified as related to a TL emission on the UV range [30]. Among the 14 TL peaks observed consistently by Lapraz and Baumer [30], in the collection of examined samples irradiated with X-rays at 77 K, three of which above room temperature are at positions very similar to our sample T_m: 360 ± 15 K, 445 ± 15 K and 545 ± 15 K, at 0.5 K/s. In addition, the same authors attribute part of the TL emission of Brazilian natural fluorapatites to activators such as Mn^{2+}, Ce^{3+} and Eu^{2+}. Furthermore, a radiation induced center was identified by Bertel et al. [48] in natural fluorapatite samples exposed to uranium. This center is defined as H(II) and is formed by an O^{2-} along with a hole occupying an F^- site.

Fig. 7 shows that the area under the TL peaks of the fluorapatite sample increases as a function of the radiation dose. It was possible to verify in this analysis a linear relationship between the dose and the area under each peak. The performed linear fits seem adequate, according to the coefficient of determination (R^2). Polymeris et al. [36] also identified that a linear behavior of the integral TL (sum of TL peaks II and III) occurs as a function of the dose (0.5 Gy up to almost 1000 Gy).

Table 2 shows the parameters of the linear best fit. The behavior of the position of each peak (T_m) as a function of the radiation dose is shown in Fig. 8, where we conclude that there is no variation in T_m in the studied dose range (1–5 Gy), suggesting a first-order kinetics.

A study of the TL kinetics to obtain information about the trapping mechanism was performed. The TL peaks were characterized using the T_m x T_{stop} method proposed by Mckeever [49], which consists in verifying the number, as well as the position of individual peaks present in complex thermoluminescent curves. To carry out this characterization, the sample previously irradiated to 1 Gy was heated (at 1 K/s) to a T_{stop} temperature, being quickly cooled to room temperature. Then, the sample was reheated to check the remaining TL curve. From this curve, the temperature position of each peak (T_m) is checked. This process was repeated several times, increasing the T_{stop} temperature in steps of 5 K, between temperatures 273–623 K. A plot of the peak temperatures in function of T_{stop} is shown in Fig. 9.

In the T_m x T_{stop} analysis, for a first-order kinetics process, a plateau is expected, meaning that T_m does not change as T_{stop} increases, up to the

Table 2
Parameters resulting from the linear fit to the data of area under the TL curve as a function of the dose, for peaks I, II and III.

Peaks	I	II	III
slope (x10^4 Gy^{-1})	5.97 ± 0.02	1.99 ± 0.10	5.27 ± 0.14
Intercept (x10^4)	−2.03 ± 0.07	−1.81 ± 0.32	−1.04 ± 0.44
R^2	0.9999	0.98308	0.9954

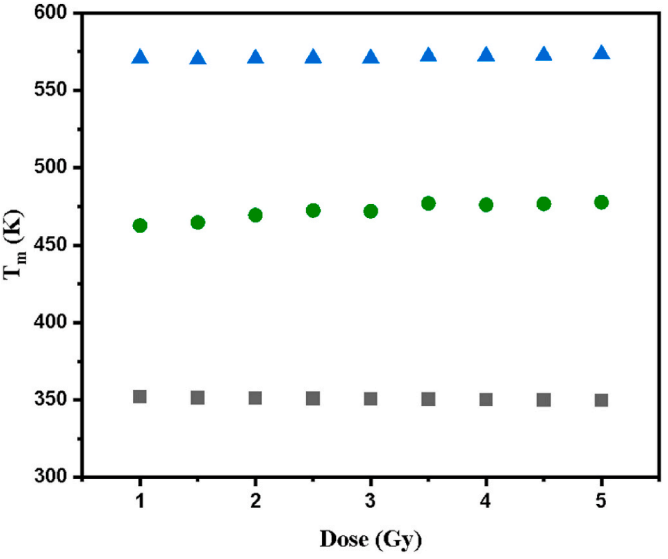

Fig. 8. Temperature position of TL peaks as a function of the radiation dose obtained for fluorapatite samples.

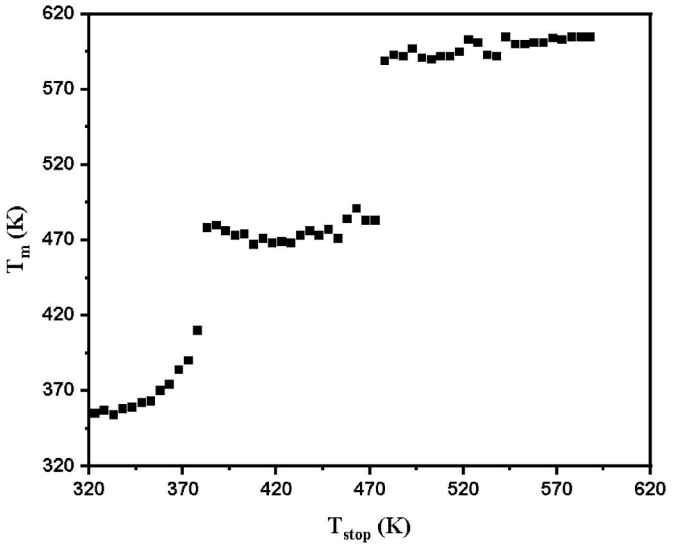

Fig. 9. T_m as function of T_{stop} for fluorapatite samples.

complete emptying of the trap connected to that particular TL peak. Whereas, for second- and general-order TL peaks, T_m x T_{stop} curve is an increasing function, that is, the maximum temperature increases as T_{stop} increases [12,49]. Therefore, according to the T_m x T_{stop} curve (Fig. 9) the TL peak I possibly obeys second or general order kinetics. The second and third peaks (II and III), on the other hand, present first order kinetics characteristics.

For a further study of the TL peaks, kinetic parameters such as kinetic order (b), activation energy (E) and frequency factor (s *or* s') were also obtained. Firstly, to determine b, the peaks were analyzed by their shape [50], through the *geometric shape factor* μ, that can be calculated by equation (1):

$$\mu = \frac{T_2 - T_m}{T_2 - T_1} = \frac{\delta}{\omega} \tag{1}$$

where T_1 and T_2 are temperatures at half the maximum TL intensity at the left and right sides of the TL peak, respectively.

From a qualitative perspective, second-order kinetic peaks are almost symmetric around T_m while first-order peaks are more asymmetric. Quantitatively, $\mu \cong 0.52$ indicates a second-order peak and $\mu \cong 0.42$ is attributed to first-order peaks. In this analysis it was not possible to apply the method to TL peak II due to its proximity to peak III, as seen in Fig. 6. Based on that, peaks I and III of our sample that had been irradiated with a dose of 1.0 Gy and heated at 1 K/s, present $\mu_I = (0.54 \pm 0.09)$ e $\mu_{III} = (0.43 \pm 0.04)$, respectively. These values indicate peak I as of second-order kinetics ($b \sim 2$) and peak III as of first-order kinetics ($b \sim 1$) [51,52].

The trap activation energy (E) can be determined by peak shape analyses, considering equation (2).

$$E_\alpha = c_\alpha \left(\frac{kT_m^2}{\alpha}\right) - b_\alpha(2kT_m) \tag{2}$$

where b_α and c_α are parameters in which α stands for the symmetry factors: $\tau = T_m - T_1$, $\delta = T_2 - T_m$ or $\omega = T_2 - T_1$ [50,52]. These parameters are calculated by equation (3).

$$\begin{aligned} c_\tau &= 1.510 + 3.0\,(\mu - 0.42) \quad b_\tau = 1.58 + 4.2\,(\mu - 0.42) \\ c_\delta &= 0.976 + 7.3\,(\mu - 0.42) \quad b_\delta = 0 \\ c_\omega &= 2.52 + 10.2\,(\mu - 0.42) \quad b_\omega = 1 \end{aligned} \tag{3}$$

Our results for the fluorapatite sample are in Table 3.

The second method applied on these analyses is based on the area of each peak, known as the *whole glow curve*. For this, the integral of each peak is calculated from different values of T smaller than T_m until the

Table 3
Summary of the results of energy (E), frequency factor (s or s') and kinetic order b for the fluorapatite sample for various analysis methods according to the text. The analysis of peak II was compromised due to its proximity to the third peak and is not included.

	Energy			
Method[a]	$E_{PS\tau}$ (eV)	$E_{PS\delta}$ (eV)	$E_{PS\omega}$ (eV)	E_{WGP} (eV)
Peak I	1.18 ± 0.04	1.09 ± 0.04	1.14 ± 0.02	0.84 ± 0.01
Peak III	0.83 ± 0.04	0.90 ± 0.04	0.86 ± 0.04	0.77 ± 0.01
	Kinetic order			
Method[a]	b_{PS}		b_{WGP}	
Peak I	2.3		1.5	
Peak III	1.0		1.0	
	Frequency Factor (*s or s'*)			
Method[a]	*WGP*			
Peak I	10^8 m^3s^{-1}			
Peak III	10^5 s^{-1}			

[a] The different methods used to obtain the values present on this table were identified by the acronyms PS (peak shape) and WGP (whole glow peak).

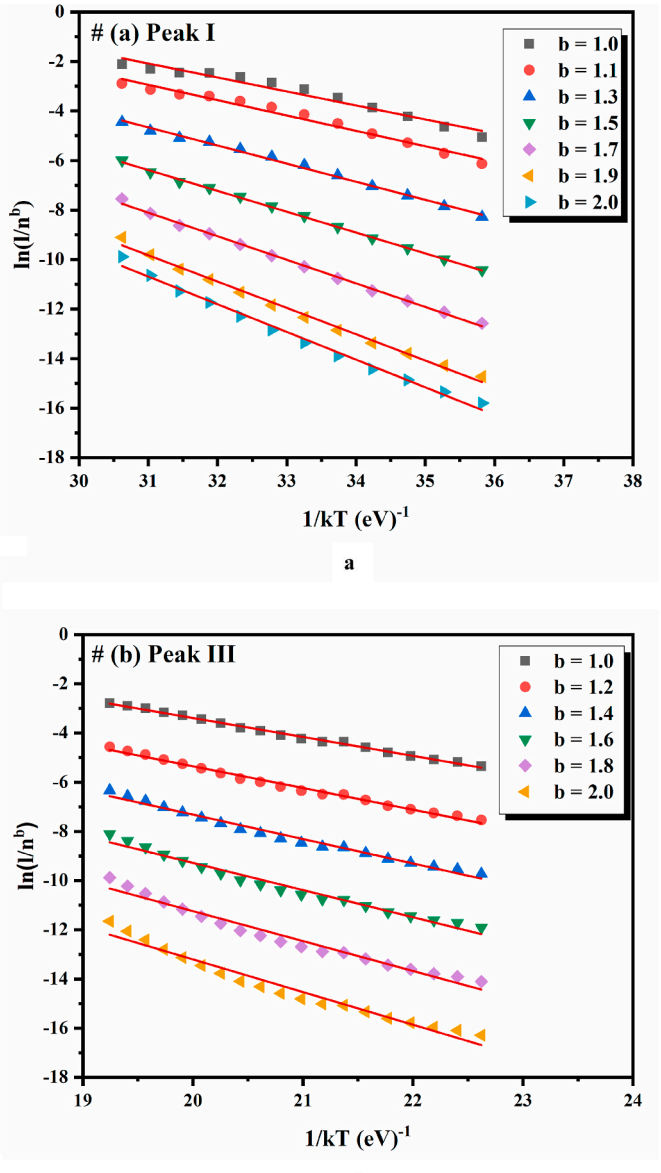

Fig. 10. $\ln(I/n^b)$ as function of 1/kT from TL glow peaks I (a) and III (b) of natural fluorapatite (exposed to 1.0 Gy beta dose) for different values of kinetic order b, with corresponding linear fittings.

final temperature of the peak. Thus, for cases in which the kinetic order is not known, it is possible to use equation (4) to obtain E:

$$\ln\left(\frac{I}{n^b}\right) = \ln\left(\frac{s'}{q}\right) - \frac{E}{kT} \quad (4)$$

where n is the area under the glow curve, I is the intensity of the emitted light at temperature T, q is the heating rate, effective frequency factor s' is the ratio of s and the concentration of available electron traps N ($s' = s/N$). The relation expressed in equation (4) makes possible to plot a graph of $ln\ (I/n^b)$ versus 1/kT, that results in a linear distribution of points by using a specific value of b referring to the kinetic order of the peak. Then, by plotting this graph for different values of b (Fig. 10) it is possible to verify the kinetic order of the peak considering the best linear fit (evaluated by the R^2 coefficient). Moreover, from the straight line fitted on the plot the slope gives the value of the activation energy (E), while the intercept is related to the frequency factor by equation (5):

$$s' = qe^{intercept} \quad (5)$$

Due to the fact that the peaks are required to be well isolated for this method, it was not possible to obtain a reliable result for peak II.

The results of energy (E), frequency factor (s or s') and kinetic order b for the fluorapatite sample for peaks I and III are summarized in Table 3. Considering the methods described in this paper, for peak I, the values of b present a variation from 1.5 to 2, indicating a general-order kinetic peak, close to a second-order kinetics. The average activation energy obtained for peak I was $\bar{E} = 1.06$ eV. Peak III shows a great coherence regarding the kinetic order by different methods ($b = 1$). The activation energy remained constant among the methods, with the average value $\bar{E} = 0.83$ eV. Finally, to best of our knowledge, this is the first time that a kinetic study is done for the thermoluminescence of fluorapatite mineral.

4. Conclusions

This work aimed to investigate the TL properties of a fluorapatite ($Ca_{10}(PO_4)_6F_2$) natural sample irradiated with beta particles. The sample was characterized chemically by SEM/EDS and structurally by XRD, being composed by fluorapatite and impurities (<1%) of S and Si. The optical absorption spectrum of the fluorapatite sample was obtained showing a wide absorption band between 500 nm and 750 nm. This band, regarding the color of the apatite, is identified in the literature due to the presence of $(MnO_4)^{3-}$ substituting for $(PO_4)^{3-}$ or alternatively due to $(SO_3)^{-}$ transitions. In addition, a peak at 740 nm was identified and related to Nd^{3+} ions according to the literature. Nonetheless, due to the limitations of the equipment, and possibly to the area of the sample that was analyzed, the chemical analysis by SEM/EDS did not indicate the presence of manganese or rare earths. The Raman spectrum shows the four vibrational modes related to $(PO_4)^{3-}$ and a peak ~ 1103 cm^{-1} that can be related to $(CaO_3)^{2-}$ vibrations. The TL glow curve showed 3 peaks located around T_m ~350 K (I), ~470 K (II) and ~570 K (III). The peak positions are constant with each dose from 1 to 5 Gy. From the two different methods used for the kinetic study, it was possible to identify that peak I shows second-order kinetic (b ~2) and energy $\bar{E}$ ~1.06 eV. Peak III obeys first-order kinetic (b ~1) with activation energy $\bar{E}$ ~0.83 eV. The analysis of peak II was compromised due to its low intensity and the proximity to peak III. However, considering the T_m - T_{stop}, peak II possibly obeys a first-order kinetics. Finally, the dose-response, from 1 to 5 Gy of beta radiation, is linear for all TL glow peaks.

Credit author statement

G. P. S. Silva: Investigation, Formal analysis, Data Curation, Writing - Original Draft, Writing-Review&Editing. M. C. S. Nunes: Investigation, Formal analysis, Data Curation, Writing - Original Draft, Writing-Review&Editing. C. Ulsen: Investigation, Data Curation, Writing-Review&Editing. R. Kunzel: Investigation, Data Curation, Writing-Review&Editing. E. M. Yoshimura: Resources, Supervision, Writing-Review&Editing. N. M. Trindade: Conceptualization, Methology, Validation, Writing - Original Draft, Writing-Review&Editing, Supervision.

Declaration of competing interest

The authors declare that they have no known competing financial interests or personal relationships that could have appeared to influence the work reported in this paper.

Acknowledgments

G.P.S. Silva (#2019/15599-1) and M.C.S Nunes (#2018/16894-4) are grateful to São Paulo Research Foundation (FAPESP). N.M. Trindade is grateful to FAPESP, grant #2019/05915-3 and IFSULDEMINAS/IFSP, grant #01/2020. E.M. Yoshimura thanks National Council for Scientific and Technological Development (CNPq) – Brazil, grant #306843/2018-8. The authors are grateful to PhD. Henrique Kahn (Polytechnic School, USP) for supplying the samples; geologists Renato Contessotto and Marco Timich (Technological Characterization Laboratory, LCT-USP) for support in XRD and SEM analysis.

References

[1] M. Pasero, A.R. Kampf, C. Ferraris, I.V. Pekov, J. Rakovan, T.J. White, Nomenclature of the apatite supergroup minerals, Eur. J. Mineral 22 (2010) 163–179, https://doi.org/10.1127/0935-1221/2010/0022-2022.
[2] F.F. Vieira, Caracterização e tratamento térmico das fluorapatitas gemológicas de Sumé-Paraíba, Universidade Federal de Campina Grande, 2017.
[3] W. Ritter, T.D. Maerk, Absorption spectroscopy of the annealing of absorbing defects in natural fluorapatite. Radiat. Eff. Defects Solids, 1983, pp. 185–191, https://doi.org/10.1080/00337578308220672.
[4] J.M. Hughes, M. Cameron, K.D. Crowley, Crystal structures of natural ternary apatites: solid solution in the $Ca_5(PO_4)_3X$ (X=F, OH, Cl) system, Am. Mineral. 75 (1990) 295–304.
[5] R.T. Downs, K.L. Bartelmehs, G. V Gibbs, Interactive software for calculating and displaying X-ray or neutron powder diffractometer patterns of crystalline materials, Am. Mineral. 78 (1993) 104–107.
[6] N. Leroy, E. Bres, D.B. Jones, S. Downes, Structure and substitutions in fluorapatite, Eur. Cell. Mater. 2 (2001) 36–48, https://doi.org/10.22203/eCM.v002a05.
[7] J.M. Hughes, J. Rakovan, The crystal structure of apatite, $Ca_5(PO_4)_3(F,OH,Cl)$, Rev. Mineral. Geochem. 48 (2002) 1–12, https://doi.org/10.2138/rmg.2002.48.1.
[8] M.C.M. de Toledo, V.P. Pereira, A variabilidade de composição da apatita associada a carbonatitos, Rev. Do Inst. Geológico. 22 (2001) 27–64, https://doi.org/10.5935/0100-929x.20010002.
[9] M.J. Kohn, J. Rakovan, J.M. Hughes, Phosphates: Geochemical, Geobiological and Materials Importance, 48th ed., Mineralogical Society of America and Geochemical Society, 2002.
[10] J. Roman-Lopez, V. Correcher, J. Garcia-Guinea, P. Prado-Herrero, T. Rivera, I. B. Lozano, Effect of the chemical impurities on the luminescence emission of natural apatites, Spectrochim. Acta Part A Mol. Biomol. Spectrosc. 126 (2014) 142–147, https://doi.org/10.1016/j.saa.2014.01.128.
[11] G.A. Waychunas, Apatite luminescence, Rev. Mineral. Geochem. 48 (2002) 701–742, https://doi.org/10.2138/rmg.2002.48.19.
[12] S.W.S. McKeever, Thermoluminescence of Solids, Cambridge University Press, Cambridge, 1985, https://doi.org/10.1017/cbo9780511564994.
[13] J.M. Kalita, G. Wary, Thermoluminescence Properties of Minerals and Their Application, LAP LAMBERT Academic Publishing, Saarbrucken, Germany, 2016.
[14] A.J.J. Bos, Theory of thermoluminescence, Radiat. Meas. 41 (2006) S45–S56, https://doi.org/10.1016/j.radmeas.2007.01.003.
[15] W.F. Hornyak, R. Chen, A. Franklin, Thermoluminescence characteristics of the 375 °C electron trap in quartz, Phys. Rev. B 46 (1992) 8036–8049, https://doi.org/10.1103/PhysRevB.46.8036.
[16] R. Kibar, J. Garcia-Guinea, A. Çetin, S. Selvi, T. Karal, N. Can, Luminescent, optical and color properties of natural rose quartz, Radiat. Meas. 42 (2007) 1610–1617, https://doi.org/10.1016/j.radmeas.2007.08.007.
[17] F.O. Ogundare, M.L. Chithambo, Thermoluminescence kinetic analysis of quartz with a glow peak that shifts in an unusual manner with irradiation dose, J. Phys. D Appl. Phys. 40 (2007) 247–253.
[18] F. Preusser, M.L. Chithambo, T. Götte, M. Martini, K. Ramseyer, E.J. Sendezera, G. J. Susino, A.G. Wintle, Quartz as a natural luminescence dosimeter, Earth Sci. Rev. 97 (2009) 184–214, https://doi.org/10.1016/j.earscirev.2009.09.006.
[19] Y.A. Abdel-Razek, Thermoluminescence dosimetry using natural calcite, J. Taibah Univ. Sci. 10 (2016) 286–295, https://doi.org/10.1016/j.jtusci.2015.08.002.
[20] J.F. de Lima, M.E.G. Valerio, E. Okuno, Thermally assisted tunneling: an alternative model for the thermoluminescence process in calcite, Phys. Rev. B 64 (2001) 14105, https://doi.org/10.1103/PhysRevB.64.014105.

[21] V. Correcher, J. Garcia-Guinea, L. Sanchez-Muñoz, T. Rivera, Luminescence characterization of a sodium-rich feldspar, Radiat. Eff. Defect Solid 162 (2007) 709–714, https://doi.org/10.1080/10420150701482063.
[22] A. Pandya, S.G. Vaijapurkar, P.K. Bhatnagar, Radiation dosimetry by potassium feldspar, Bull. Mater. Sci. 23 (2000) 155–158, https://doi.org/10.1007/bf02706559.
[23] A.P. Melo, M.E.G. Valerio, L.V.E. Caldas, Thermoluminescent characteristics of mineral samples acquired as jade, Nucl. Instrum. Methods Phys. Res. Sect. B Beam Interact. Mater. Atoms 218 (2004) 198–201, https://doi.org/10.1016/j.nimb.2003.12.058.
[24] S. Watanabe, N.F. Cano, L.S. Carmo, R.F. Barbosa, J.F.D. Chubaci, High- and very-high-dose dosimetry using silicate minerals, Radiat. Meas. 72 (2015) 66–69, https://doi.org/10.1016/j.radmeas.2014.11.004.
[25] S.L. Dardengo, M.C.S. Nunes, C. Ulsen, E.M. Yoshimura, N.M. Trindade, Investigação da termoluminescência de alexandrita ($BeAl_2O_4$: Cr^{3+}), Brazilian J. Radiat. Sci. 8 (2020), https://doi.org/10.15392/bjrs.v8i2.1215.
[26] N.M. Trindade, H. Kahn, E.M. Yoshimura, Thermoluminescence of natural $BeAl_2O_4$:Cr^{3+} Brazilian mineral: preliminary studies, J. Lumin. 195 (2018) 356–361, https://doi.org/10.1016/j.jlumin.2017.11.057.
[27] N.M. Trindade, M.R. da Cruz, H. Kahn, L.G. Jacobsohn, E.M. Yoshimura, Thermoluminescence and radioluminescence of alexandrite mineral, J. Lumin. 206 (2019) 455–461, https://doi.org/10.1016/j.jlumin.2018.10.114.
[28] M.C.S. Nunes, L.S. Lima, E.M. Yoshimura, L.V.S. França, O. Baffa, L.G. Jacobsohn, A.L.M.C. Malthez, R. Kunzel, N.M. Trindade, Characterization of the optically stimulated luminescence (OSL) response of beta-irradiated alexandrite-polymer composites, J. Lumin. 226 (2020) 117479, https://doi.org/10.1016/j.jlumin.2020.117479.
[29] N.M. Trindade, M.R. Cruz, E.M. Yoshimura, Correlation between thermoluminescence and optically stimulated luminescence responses of natural alexandrite, Appl. Radiat. Isot. 166 (2020) 109402, https://doi.org/10.1016/j.apradiso.2020.109402.
[30] D. Lapraz, A. Baumer, Thermoluminescent properties of synthetic and natural fluorapatite,$Ca_5(PO_4)_3F$, Phys. Status Solidi 80 (1983) 353–366, https://doi.org/10.1002/pssa.2210800139.
[31] N.C. Tsirliganis, G.S. Polymeris, G. Kitis, V. Pagonis, Dependence of the anomalous fading of the TL and blue-OSL of fluorapatite on the occupancy of the tunnelling recombination sites, J. Lumin. 126 (2007) 303–308, https://doi.org/10.1016/j.jlumin.2006.07.011.
[32] N. Tsirliganis, G. Polymeris, Z. Loukou, G. Kitis, Anomalous fading of the TL, Blue-SL and IR-SL signals of fluorapatite, Radiat. Meas. 41 (2006) 954–960, https://doi.org/10.1016/j.radmeas.2006.04.024.
[33] G.S. Polymeris, I.K. Sfampa, M. Niora, E.C. Stefanaki, L. Malletzidou, V. Giannoulatou, V. Pagonis, G. Kitis, Anomalous fading in TL, OSL and TA – OSL signals of Durango apatite for various grain size fractions; from micro to nano scale, J. Lumin. 195 (2018) 216–224, https://doi.org/10.1016/j.jlumin.2017.11.034.
[34] G. Kitis, G.S. Polymeris, V. Pagonis, N.C. Tsirliganis, Anomalous fading of OSL signals originating from very deep traps in Durango apatite, Radiat. Meas. 49 (2013) 73–81, https://doi.org/10.1016/j.radmeas.2012.11.011.
[35] G. Kitis, G.S. Polymeris, V. Pagonis, N.C. Tsirliganis, Thermoluminescence response and apparent anomalous fading factor of Durango fluorapatite as a function of the heating rate, Phys. Status Solidi Appl. Mater. Sci. 203 (2006) 3816–3823, https://doi.org/10.1002/pssa.200622197.
[36] G.S. Polymeris, N. Tsirliganis, Z. Loukou, G. Kitis, A comparative study of the anomalous fading effects of TL and OSL signals of Durango apatite, Phys. Status Solidi 203 (2006) 578–590, https://doi.org/10.1002/pssa.200521347.
[37] G. Kitis, P. Bousbouras, C. Antypas, S. Charalambous, Anomalous fading in apatite, Int. J. Radiat. Appl. Instrum. Nucl. Tracks Radiat. Meas. 18 (1991) 61–65, https://doi.org/10.1016/1359-0189(91)90093-W.
[38] G.S. Polymeris, V. Giannoulatou, I.K. Sfampa, N.C. Tsirliganis, G. Kitis, Search for stable energy levels in materials exhibiting strong anomalous fading: the case of apatites, J. Lumin. 153 (2014) 245–251, https://doi.org/10.1016/j.jlumin.2014.03.041.
[39] M. Miler, B. Mirtič, Accuracy and precision of EDS analysis for identification of metal-bearing minerals in polished and rough particle samples, Geologija 56 (2013) 5–17, https://doi.org/10.5474/geologija.2013.001.
[40] H.B. Ribeiro, K.J. Guedes, M.V.B. Pinheiro, S. Greulich-Weber, K. Krambrock, About the blue and green colours in natural fluorapatite, Phys. Status Solidi 2 (2005) 720–723, https://doi.org/10.1002/pssc.200460274.
[41] L.G. Gilinskaya, R.I. Mashkovtsev, Blue and green centers in natural apatites by ERS and optical spectroscopy data, J. Struct. Chem. 36 (1995) 76–86, https://doi.org/10.1007/BF02577752.
[42] J.M. Hughes, A. Ertl, H.-J. Bernhardt, G.R. Rossman, J. Rakovan, Mn-rich fluorapatite from Austria: crystal structure, chemical analysis, and spectroscopic investigations, Am. Mineral. 89 (2004) 629–632, https://doi.org/10.2138/am-2004-0417.
[43] E. Cantelar, G. Lifante, T. Calderón, R. Meléndrez, A. Millán, M. Alvarez, M. Barboza-Flores, Optical characterisation of rare earths in natural fluorapatite, J. Alloys Compd. 323–324 (2001) 851–854, https://doi.org/10.1016/S0925-8388(01)01159-8.
[44] G. Leroy, N. Leroy, G. Penel, C. Rey, P. Lafforgue, E. Bres, Polarized micro-Raman study of fluorapatite single crystals, Appl. Spectrosc. 54 (2000) 1521–1527, https://doi.org/10.1366/0003702001948448.
[45] A. Antonakos, E. Liarokapis, T. Leventouri, Micro-Raman and FTIR studies of synthetic and natural apatites, Biomaterials 28 (2007) 3043–3054, https://doi.org/10.1016/j.biomaterials.2007.02.028.
[46] G. Penel, G. Leroy, C. Rey, E. Bres, MicroRaman spectral study of the PO_4 and CO_3 vibrational modes in synthetic and biological apatites, Calcif. Tissue Int. 63 (1998) 475–481, https://doi.org/10.1007/s002239900561.
[47] D. Ekendahl, L. Judas, L. Sukupova, OSL and TL retrospective dosimetry with a fluorapatite glass-ceramic used for dental restorations, Radiat. Meas. 58 (2013) 138–144, https://doi.org/10.1016/j.radmeas.2013.01.001.
[48] E. Bertel, W. Ritter, E. Bertagnolli, T.D. Märk, Fission-damage-induced color centers in apatite, Phys. Rev. B 27 (1983) 3730–3734, https://doi.org/10.1103/PhysRevB.27.3730.
[49] S.W.S. Mckeever, On the analysis of complex thermoluminescence. Glow-curves: resolution into individual peaks, Phys. Status Solidi 62 (1980) 331–340, https://doi.org/10.1002/pssa.2210620139.
[50] V. Pagonis, G. Kitis, C. Furetta, Numerical and Practical Exercises in Thermoluminescence, first ed., Springer-Verlag, New York, 2006 https://doi.org/10.1007/0-387-30090-2.
[51] R. Chen, On the calculation of activation energies and frequency factors from glow curves, J. Appl. Phys. 40 (1969) 570–585, https://doi.org/10.1063/1.1657437.
[52] C.M. Sunta, Unraveling Thermoluminescence, Springer India, 2015, https://doi.org/10.1007/978-81-322-1940-8.